Experimental demonstration of the effect of frequency mapping on performance in an SOA-based C-RAN architecture based on the AIFoF technology for 5G communications

Mahdi Kasmi, Pascal Morel, Mihai Telescu, Vincent Choqueuse, Noël Tanguy, Stéphane Azou

Experimental demonstration of the effect of frequency mapping on performance in an SOA-based C-RAN architecture based on the AIFoF technology for 5G communications

Mahdi Kasmi, Pascal Morel, Mihai Telescu, Vincent Choqueuse, Noël Tanguy, and Stéphane Azou, *Senior Member, IEEE*

***Abstract*—In order to mitigate second-order intermodulation distortion products, induced by the interaction between the Mach-Zehnder modulator, the photodiode and the semiconductor optical amplifier in an optical fronthaul fifth generation architecture, an optimized intermediate frequency configuration has been proposed and analytically investigated. It has been experimentally validated through the transmission of three orthogonal frequency division multiplexing bands of 200 MHz through 18.3 km of single-mode fiber, using the analog intermediate frequency signal over fiber technology. Results show the optimized intermediate frequency configuration leads to an error vector magnitude improvement for the 4 and 16-QAM cases.**

***Index Terms*—Analog intermediate frequency signal over fiber, fifth generation, nonlinearities, orthogonal frequency division multiplexing, semiconductor optical amplifier, second-order intermodulation distortions.**

I. INTRODUCTION

To provide the three service categories (i.e. enhanced mobile broadband, massive machine-type communications and ultra-reliable and low latency communications), the fifth generation (5G) is supposed to deliver higher data rates up to 10 Gb/s with lower latencies, less than 1 ms. In order to meet these stringent requirements, a novel network architecture, called centralized/cloud radio access network (C-RAN), has been presented [1].

This work was funded by the Brittany Region under the grant number SAD 2021 PROOF-Tx (21007843) as well as by the Departmental Council of Finistère within the framework of the APRE program (project 2021 PROOF-Tx). *(Corresponding author: Mahdi Kasmi).*

M. Kasmi, P. Morel, V. Choqueuse and S. Azou are with the Brest National School of Engineering (ENIB), Lab-STICC, CNRS, UMR 6285 CS 73862 – 29238, Brest Cedex 3, France (e-mail: mahdi.kasmi@enib.fr; morel@enib.fr; choqueuse@enib.fr; azou@enib.fr).

M. Telescu and N. Tanguy are with the University of Brest, Lab-STICC, CNRS, UMR 6285 F-29200 Brest, France (e-mail: Mihai.Telescu@univ-brest.fr; noel.tanguy@univ-brest.fr).

It is composed of distributed units (DUs) placed in the central office and shared between radio units (RUs) located at different cell sites. This mobile optical fronthaul connection between distributed and radio units was primarily based on the digital radio over fiber (D-RoF) technique using the common public radio interface (CPRI) standard. In fact, the CPRI line bit rate increases proportionally with the bandwidth (BW) and with the number of antennas [2]. To support for example three directional sectors in 5G technologies, the required CPRI total bit rate, over 200 MHZ of BW with 64x64 MIMO, reaches 2.4 Tb/s [3]. Thus, the common public radio interface cannot scale to the 5G requirements since it imposes a high penalty in terms of data rate and latency. Therefore, new alternatives have been put forward such as the enhanced CPRI based on the functional split and also the analog RoF (A-RoF) [4], where an analog radio frequency (RF) or intermediate frequency (IF) signal is carried out through the fronthaul link.

The A-RoF can be either analog-domain radio frequency signal over fiber (ARFoF) or analog intermediate frequency signal over fiber (AIFoF). With the ARFoF, the digital baseband signal is transformed to analog form and up-converted to the desired radio frequency f_{RF} before being transmitted via the optical link. Thus, the spectral efficiency is improved by avoiding the quantization and the oversampling at the multiple RUs [5], needed for the digital radio-over-fiber systems. Besides, by operating with much simpler radio units designed for basic radio frequency functions, the analog radio-over-fiber technology can significantly achieve cost savings and reduce power consumption as there is no use of expensive and energy-consuming analog to digital/digital to analog converters at each RU. Unfortunately, however, ARFoF becomes very sensitive to nonlinear distortions at high radio frequencies, within the 5G millimeter wave band for instance.

Consequently, the AIFoF fronthauling solution is usually adopted [6]. It is based on up-converting the signal first to a smaller intermediate frequency ($f_{IF} < f_{RF}$) at the DU and then to the radio frequency by a local oscillator ($f_{RF} = f_{IF} + f_{LO}$) at the RU, as presented in Fig. 1.

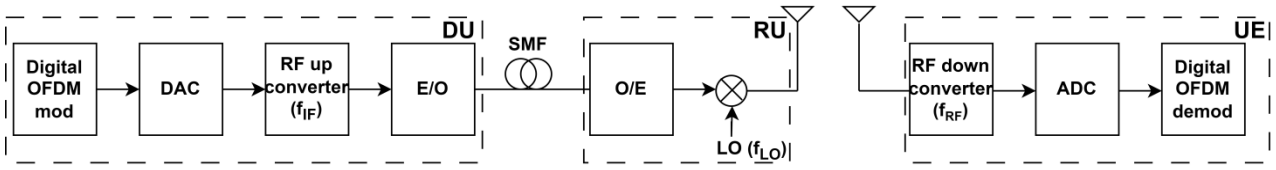

Fig. 1. Block diagram of the AIFoF technology for the fronthaul link (E/O: electrical-to-optical; O/E: optical-to-electrical).

Although it presents many merits, including the flexibility to use lower-bandwidth optical components, AIFoF is still not completely immune to nonlinearities. Among the possible nonlinear impairments, second-order and third-order nonlinear distortion products (DP2, DP3), which encompass both harmonics and intermodulation distortion products, are the most critical since they are high in amplitude and adjacent to the desired signals. So, they can therefore degrade the transmission quality.

Many works have been carried out in order to overcome these DPs, by inserting optical devices [7] or using different predistorters [8] and equalizers [9], at the expense of cost and system complexity. For this reason, researchers have proposed new techniques, instead of signal processing methods. Paper [10] presented a spectral power shaping technique to handle particularly third-order intermodulations in an IF over fiber system by redistributing the spectral signal power. Based on the transmission of 48, 72, and 144 long-term evolution-advanced (LTE-A) bands with 64-QAM modulation and over 20 km of single-mode fiber (SMF), previous research proved the efficiency of the intermediate frequency spacing optimization scheme [11] and the octave-confined frequency plan scheme [12] in avoiding DP2s.

By contrast, in this work, we focus specifically on the mitigation of second-order distortion products, with a scenario supporting bandwidths of up to 200 MHz per band. Indeed, in contrast with LTE's 20 MHz BW, the 5G New Radio supports up to 100 MHz in the frequency range 1 (FR1: sub 6 GHz) and up to 400 MHz in the frequency range 2 (FR2: above 24 GHz), according to the 3rd Generation Partnership Project (3GPP) specifications [13]. These higher bandwidths are based on a scalable OFDM numerology in terms of number of antenna channels and subcarrier spacings. According to [11], the frequency spacing has to be three times the bandwidth, which degrades the bandwidth efficiency. For this reason, we propose in the present paper an updated frequency mapping method based on the computation of the optimized intermediate frequency within a small fixed frequency spacing equal to the sum of the signal BW (i.e. 200 MHz) and the 10 % guard-band (GB) (i.e. 20 MHz), as was the case with LTE.

Besides, we work in a more challenging context where DP2s are not only induced by the interaction between the laser and the fiber, as reported in [11], but also due to the nonlinear effects caused by the booster amplifier. Indeed, the fiber attenuation lowers the signal power and induces errors on the receiver side. In order to maintain the signal quality over the fronthaul network, we propose the use of a semiconductor amplifier (SOA) [14] as a booster amplifier, in the C-RAN architecture and demonstrate it is a viable option. As discussed in previous studies, semiconductor amplifiers present many attractive features including a lower size and cost in comparison with other amplifiers (e.g. Erbium doped fiber amplifiers (EDFA) and Raman amplifiers), while operating within a wide wavelength range (i.e. 1280-1650 nm).

To the best of our knowledge, the mitigation of second-order intermodulations, based on a novel proposed frequency mapping method in a 5G SOA-based orthogonal frequency division multiplexing (OFDM) system, has not been analyzed or experimentally validated before. In order to focus on DP2s arising from the fronthaul link between the distributed and radio units, we experimentally study the multiband OFDM transmission over the SMF portion and we assume the wireless link between the radio unit and the user equipment (UE) to be ideal.

This paper is organized as follows: section II describes the numerical analysis that enables to derive the optimized IF configuration. In section III, experimental results are presented in order to validate the effect of the frequency mapping on performance. Finally, Section IV presents some conclusions.

II. NUMERICAL DERIVATION OF AN OPTIMIZED IF CONFIGURATION FOR SOA-BASED OFDM SYSTEMS

A. Single-drive Mach-Zehnder modulator model

In optical communication systems, nonlinearities come essentially from the fiber and all the electro-optical components. In our scenario, the nonlinear effects of the SMF can be neglected as the considered length is relatively short. However, the Mach-Zehnder modulator (MZM), the photodiode (PD) and the SOA are major sources of nonlinearities at high powers, especially in the presence of non-constant envelope signals with a high peak to average power ratio (PAPR) such as OFDM. When the SOA is not considered, the output current signal of the photodiode i_{PD} is proportional to the MZM output optical power P_{MZM}. In a quasi-linear channel model, it can be approximated as

$$i_{PD}(t) \propto R P_{MZM}(t), \quad (1)$$

where R is the photodiode responsivity. P_{MZM} can be expressed as [15]:

$$P_{MZM}(t) = |E_{MZM}(t)|^2 = \alpha_m P_L \cos^2\left(\frac{\pi}{2V_\pi} V(t)\right), \quad (2)$$

where E_{MZM} is the MZM output field, α_m is the modulator optical insertion loss coefficient, P_L is the continuous wave (CW) laser power and V_π is the half-wave voltage. $V(t)$ denotes the input voltage which can be expressed as a function of the DC biasing voltage V_{DC}, the peak-to-peak voltage V_{pp} and

the normalized OFDM signal $d(t)$ as:

$$V(t) = V_{DC} + V_{pp}d(t). \quad (3)$$

To operate in the linear regime and to optimize the performances, the MZM bias is usually set to the quadrature point (i.e. $V_{DC} = \frac{3}{2}V_\pi$). Thus, (2) becomes after simplification:

$$P_{MZM}(t) = \alpha_m \frac{P_L}{2}\left(1 + sin\left(\frac{\pi V_{pp}}{V_\pi}d(t)\right)\right). \quad (4)$$

Based on (4) and as illustrated in Fig. 2, the MZM power transfer function is symmetric to the operating point V_{DC}. Thus, at the photodiode output, only odd-order distortion products remain.

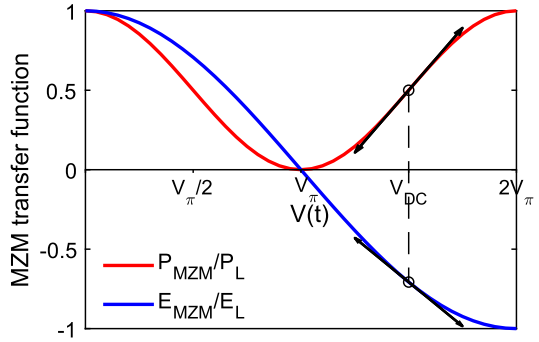

Fig. 2. Field and power transfer functions of the single-drive MZM modulator (E_L is the laser field, $\alpha_m = 1$ is assumed).

B. Analysis of second-order distortion products in an SOA-based OFDM system

As it might be hard to visualize intermodulations with several OFDM bands, we investigate them by simulating in MATLAB® a single OFDM signal composed of only two subcarriers, located at $f_1 = 0.62$ GHz and $f_2 = 1.02$ GHz. The SOA was modeled using Keysight Advanced Design System (ADS), according to a numerical model that has already been experimentally validated in [14]. As discussed previously and confirmed in Fig. 3(a), even order DPs are eliminated at the photodiode output. However, they appear in the presence of an SOA (Fig. 3 (b)). In fact, the SOA depends on E_{MZM}, which is not symmetric to V_{DC} (Fig. 2). Thus, odd- and even-order distortion products, generated at the MZM output, are amplified by the SOA and subjected to its relative odd nonlinearities. The field transfer characteristic of the MZM is disturbed by passing through the SOA and not only odd but also even-order DPs are by consequence present at the photodiode output. The second-order intermodulation distortion product $(f_2 - f_1)$ and the second harmonic $(2f_1)$ may cause particularly serious interferences as they are close to the user subcarriers and also very strong in power, as depicted in Fig. 3. Note that the theoretical and numerical values of second and third order distortion products are given in Table I.

Starting from this observation, we evaluate a more general case of n transmitted bands (B_1, B_2, ..., B_n), centered at (f_1, f_2, ..., f_n). Note that the intermediate frequency f_i of the band B_i is determined based on the frequency of its predecessor band as follows: $f_i = f_{i-1} + BW + GB$. In order to prevent all the second-order distortion products, we need to focus on the DPs $(f_n - f_1)$ and $(2f_1)$. By moving them away from the desired carrier frequencies, we avoid as well all the other second-order distortion products, as they represent the closest components, as observed in Fig. 3 for the case of two subcarriers. Thus, we have to solve the following inequalities (5-6),

$$f_n - f_1 + BW \leq f_1 - \frac{BW}{2} - \frac{GB}{2}, \quad (5)$$

$$2f_1 - BW \geq f_n + \frac{BW}{2} + \frac{GB}{2}. \quad (6)$$

By adding $f_1 - \frac{BW}{2} + \frac{GB}{2}$ to both sides of (5), (5) and (6) become identical and leads then to the unique solution (7), expressing the condition on the frequency of the first band f_1 that must be fulfilled in order to ensure no second harmonic or second-order intermodulation interference:

$$f_1 \geq \left(n + \frac{1}{2}\right)BW + \left(n - \frac{1}{2}\right)GB. \quad (7)$$

For $n = 3$, f_1 should be greater than or equal to $f_{limit} = 0.75$ GHz. We represent in Fig. 4 the location of DPs $(f_3 - f_1)$ and $(2f_1)$, with regard to the three carrier frequencies, for two studied values of IF $f_1 = 0.6$ GHz and 0.8 GHz. Hence, we verify that when $f_1 < f_{limit}$, $(f_3 - f_1)$ and $(2f_1)$ interfere with the edge bands B_1 and B_3 (Fig. 4 (a)). Whereas, these considered distortion products are being placed away from the user bands when $f_1 \geq f_{limit}$ (Fig. 4(b)).

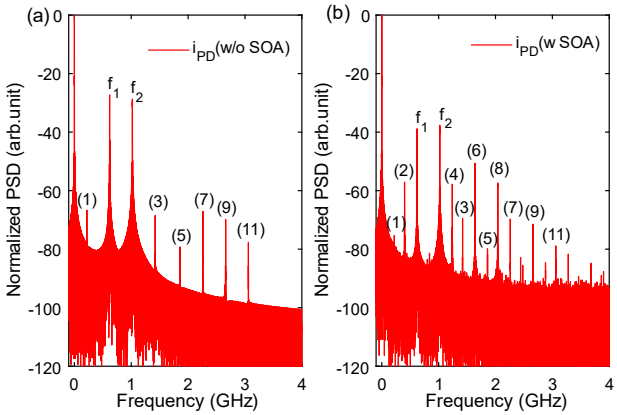

Fig. 3. Locations of intermodulation distortion products and harmonics at the output of photodiode (a) w/o SOA, and (b) w SOA, $\frac{V_{pp}}{V_\pi} = 0.5$ and $P_{in\ SOA} = 0$ dBm.

TABLE I
THEORETICAL AND NUMERICAL VALUES OF INTERMODULATION DISTORTION PRODUCTS /HARMONICS FOR TWO OFDM SUBCARRIERS CASE ($f_1 = 0.62$, $f_2 = 1.02$ GHz)

Peak index	Theo. Val.	Num. Val. (GHz)
1	$2f_1 - f_2$	0.22
2	$f_2 - f_1$	0.40
3	$2f_2 - f_1$	1.42
4	$2f_1$	1.24
5	$3f_1$	1.86
6	$f_1 + f_2$	1.64
7	$2f_1 + f_2$	2.26
8	$2f_2$	2.04
9	$f_1 + 2f_2$	2.66
11	$3f_2$	3.06

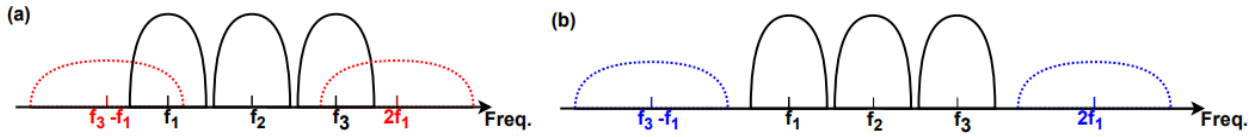

Fig. 4. Second harmonic ($2f_1$) and second intermodulation product ($f_3 - f_1$) for (a) f_1= *0.60*, f_2=*0.82*, f_3=*1.04* GHz and for (b) f_1= *0.80*, f_2=*1.02*, f_3=*1.24* GHz.

III. EXPERIMENTAL VALIDATION OF THE IMPACT OF IF MAPPING ON SYSTEM PERFORMANCE

A. Experimental setup

The experimental setup is presented by Fig. 5. Using MATLAB®, which is installed on the computer, three cyclic-prefix OFDM bands of an effective bandwidth of 200 MHz each, are generated and up converted to the desired intermediate frequencies. Each band is composed of 32 symbols, each containing 1024 subcarriers. 330 subcarriers undergo 4-QAM modulation, while the rest are nulled. The resulting multiband signal is then sent from the computer to the Keysight M8195A arbitrary waveform generator (AWG), based on a virtual instrument system architecture (VISA) connection. The resulted electrical signal is amplified by the RF amplifier module (iXblue DR-AN-20-HO driver) which has a gain of 30 dB. A 4 dB attenuator is placed before the amplifier to provide an overvoltage protection. The electro-optical conversion is afterwards performed by means of an 1550 nm external cavity laser (ECL) and a 10 Gb/s Mach-Zehnder optical intensity modulator. Note that two manual polarization controllers (PCs) are placed in front of the MZM and the SOA respectively in order to maximize the signal power on the receiver side. Before being transmitted through 18.3 km of SMF, the outputted optical signal passes through the SOA unit. The latter is composed of the SOA (INPHENIX-IPSAD1501), the temperature controller (Profile ThorLabs TED200) and the laser diode controller (Thorlabs LDC 210C) to adjust the bias current. Using a splitter, 10% of the signal is received either by the powermeter or the APEX AP2683A optical complex spectrum analyzer (OCSA). The remaining 90% of the signal is converted back to the electrical domain by a 12.5 GHz photodiode (PD) and sent to the oscilloscope (Agilent Technologies DSO-X 4154A). Finally, through the vector signal analysis (VSA) software, the computer could interact with the oscilloscope in order to save a trace of the received signal, which can be analyzed on the computer through MATLAB®. Thus, received bands are down-converted to baseband, synchronized, equalized and demodulated in order to recover the data bits and to evaluate system performance.

Table II summarizes the principal parameters for this experimental setup. The computer portion consisting of the construction of the transmitted OFDM signals (i.e. OFDM modulation and RF up conversion) and the processing of the received signals (i.e. RF down conversion, low-pass filtering, synchronization, equalization and demodulation) were described in detail in our last publication [16].

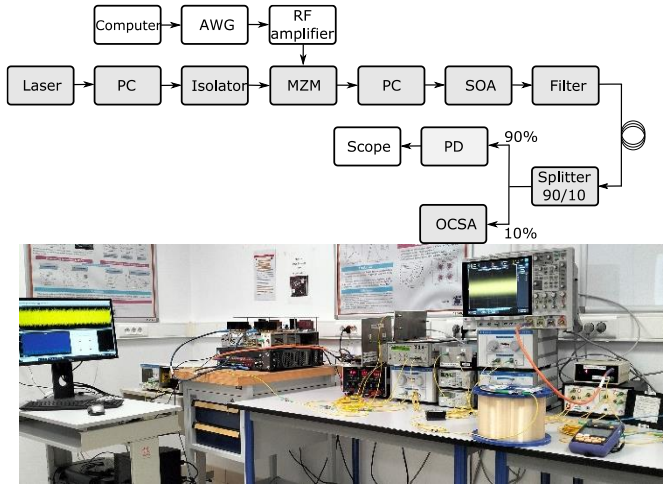

Fig. 5. Experimental setup of the SOA based OFDM multiband system.

TABLE II
EXPERIMENT PARAMETERS

Parameters	Values
Nb of OFDM bands, BW per band, Nb of symbols	3, 200 MHz, 32
Nb of data subcarriers, IFFT size, cyclic prefix	330, 1024, 64
Laser λ	1550 nm
MZM V_π, V_{DC}	6 V, 1.5 V_π
SMF L_{SMF}, α	18.3 km, 0.2 dB/km
SOA I_{bias}	150 mA
AWG sample rate	60 GSa/s
Oscilloscope sample rate	5 GSa/s

B. Experimental results and discussions

The average error vector magnitude (EVM) of the three bands, centered at $f_1 = 0.60$, $f_2 = 0.82$ and $f_3 = 1.04$ GHz, is first evaluated at different input laser powers P_L and for various values of peak-to-peak voltage. A smaller V_{pp} value induces a lower power of the OFDM modulating signal and generates then a reduced signal to noise ratio (SNR) value. For this reason, at $P_L = -5$ dBm, especially with $V_{pp} = 0.3V_\pi$ and $V_{pp} = 0.5V_\pi$, high EVMs are observed in Fig. 6(a) (33.76% and 20.45% respectively), since the corresponding signals are more vulnerable to the amplified spontaneous emission noise effects of the SOA which are dominant in this region.

By increasing P_L, the optical SNR (OSNR) is improved. The EVM diminishes significantly and reaches 7.41% with $V_{pp} = 0.5V_\pi$, at $P_L = 5$ dBm. Fig. 6(b) depicts the power spectral density (PSD) of the received electrical signals at 0 dBm, and confirms the fact of obtaining higher signal powers at the receiver side, with a greater $\frac{V_{pp}}{V_\pi}$ value. However, we notice that

the EVM increases again with $V_{pp} = V_\pi$ at $P_L = 10$ dBm, since the SOA nonlinear effects start to appear at higher input powers and become even more prominent with larger V_{pp} values. Using the APEX AP2683A OCSA, characterized by a noise floor limitation of -77 dBm, we display in Fig. 7 the optical OFDM multiband signal with $V_{pp} = V_\pi$ at 0 dBm of laser power.

In Fig. 8(a), we present the EVM for the three bands at $P_L = 10$ dBm, with $V_{pp} = V_\pi$. One notices that higher EVM values are obtained for the first and third bands in comparison to the second one. According to this IF configuration, the second intermodulation product ($f_3 - f_1 = 0.44$ GHz) and the second harmonic product ($2f_1 = 1.2$ GHz) are located near the first and third bands respectively, as illustrated by Fig. 4(a). Thus, these nonlinear distortion products cause interference to these edge bands and impact dramatically their EVM levels. Therefore, we reevaluate our experimental setup, according to a second IF configuration ($f_1 = 0.80$, $f_2 = 1.02$, $f_3 = 1.24$ GHz), that respects the condition (i.e. $f_1 \geq 0.75$ GHz, for $n = 3$) defined by our established formula, in order to avoid second order DPs. In this second scenario presented in Fig. 8, almost similar EVM values are achieved for the three bands. This EVM improvement for the first and third bands (from 11.8% to 6.8% and from 8.7% to 6.9% respectively) is attributed to the fact of choosing an intermediate frequency f_1 that keeps all the second-order intermodulation distortion products and harmonics far enough from B_1 and B_3, as shown in Fig. 4(b).

We then try to validate these experimental results in the case of 16-QAM. As reported previously with 4-QAM, B_1 and B_3 present similarly worse EVM performances than B_2, based on the first IF configuration. Indeed, Fig. 9(a) indicates an EVM of 10.5% for the third band, whereas the first one reaches even a higher EVM level of 13.9%, which is beyond the EVM limit of 12.5% required by the 3GPP for 16-QAM [13]. With the second IF configuration, lower EVM levels of around 7% are attained for B_1 and B_3 and become very close to that obtained at B_2.

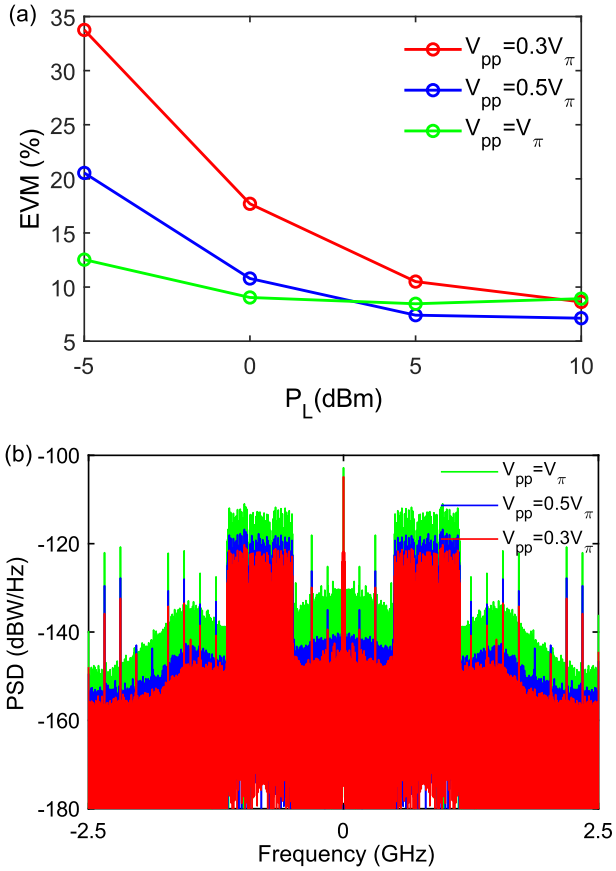

Fig. 6. (a) Average EVM vs P_L; (b) Electrical OFDM spectrum at the photodiode output for different V_{pp} values.

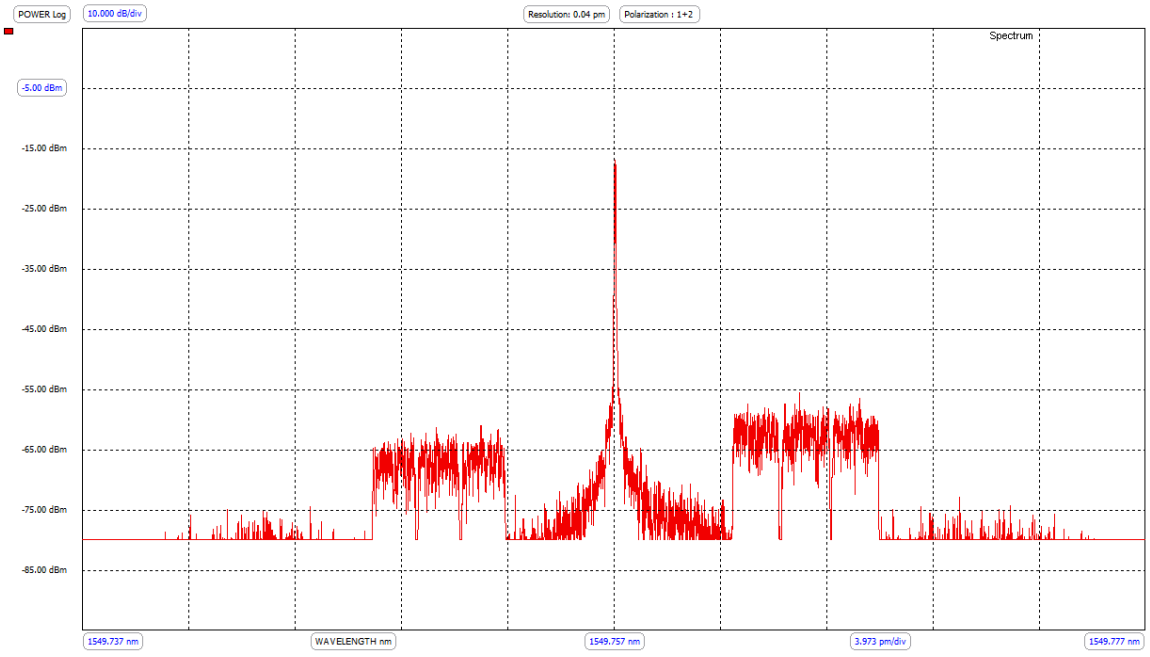

Fig. 7. Optical OFDM spectrum for $V_{pp} = V_\pi$ at $P_L = 0$ dBm.

In order to better visualize the effect of this frequency mapping on performance, we present in Fig. 8(b) and Fig. 9(b) the constellations diagrams at the receiver side of the 4-QAM 16-QAM transmitted symbols respectively, for the two different intermediate frequency configurations.

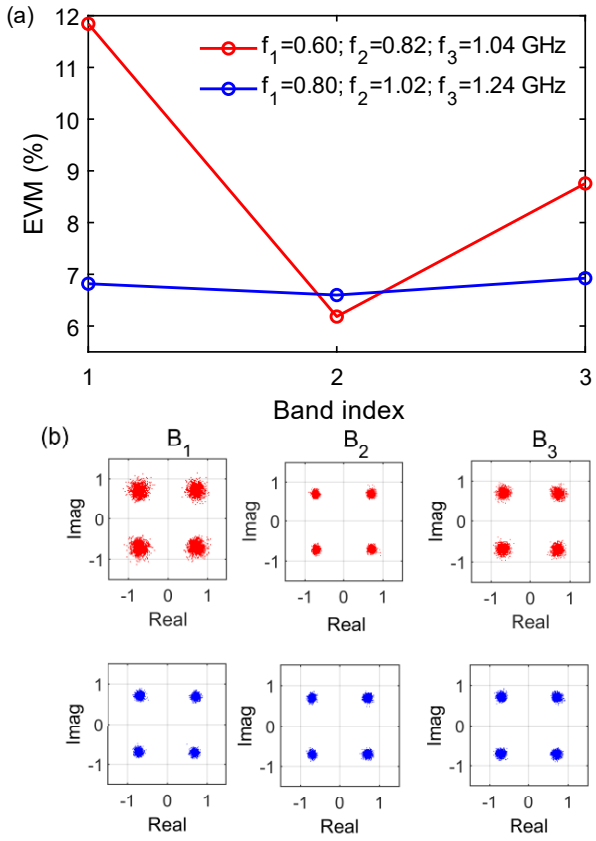

Fig. 8. (a) EVM performance for three 4-QAM-OFDM bands (b) 4-QAM constellation diagrams for the first (in red) and the second (in blue) IF configuration.

Afterwards, the EVM was examined over an extended range of input laser powers, for 4-QAM and 16-QAM modulations. At -5 dBm, almost similar EVM values are obtained for the two IF considered configurations, as depicted in Fig. 10. In fact, the SOA operates in its linear regime at very low powers, and no intermodulation products are expected. For this reason, the frequency mapping does not have any effect on EVM levels. However, with a larger laser power P_L, the SOA starts entering its nonlinear regime. Hence, intermodulation products and harmonics become present and degrade performances with an intermediate frequency $f_1 = 0.6$ GHz. By consequence, the EVM gap between the two frequency configurations appears at $P_L = 0$ dBm and becomes wider by further increasing the laser power as the nonlinear effects become stronger.

Finally, we seek to evaluate here the average EVM for other IF configurations, with 4-QAM and 16-QAM. Fig. 11 shows that the further the IF f_1 is below the frequency limit value ($f_{limit} = 0.75$ GHz) the worse the EVM becomes. In fact, by reducing f_1, the number of second-order distortion products interfering with the user bands B_1 and B_3 increases. For instance, when the bands are centered at $f_1 = 0.20$, $f_2 = 0.42$, $f_3 = 0.64$ GHz, not only $(f_3 - f_1)$ and $(2f_1)$ are problematic, as previously discussed, but also $(f_2 - f_1)$, $(f_3 - f_2)$, and $(f_1 + f_2)$ which come to impact B_1 and B_3 as well.

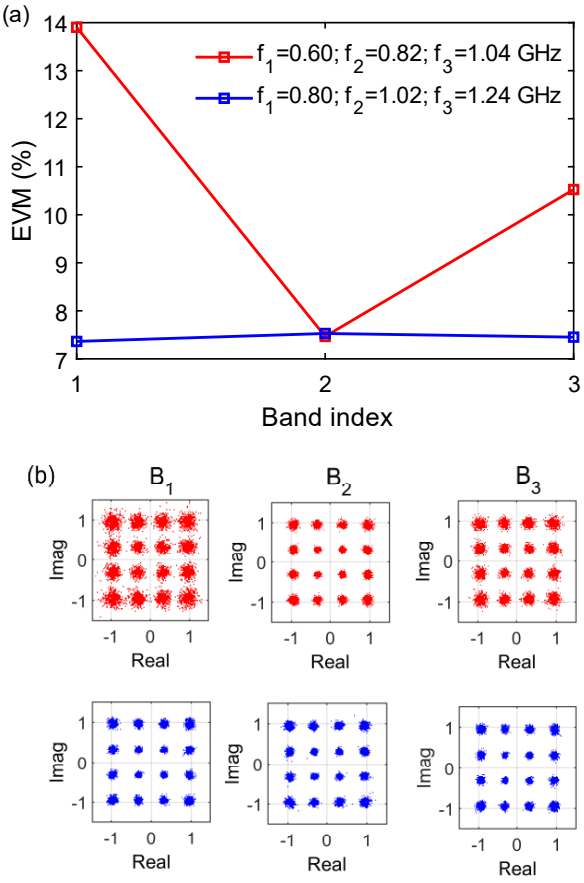

Fig. 9. (a) EVM performance for three 16-QAM OFDM bands (b) 16-QAM constellation diagrams for the first (in red) and the second (in blue) IF configuration.

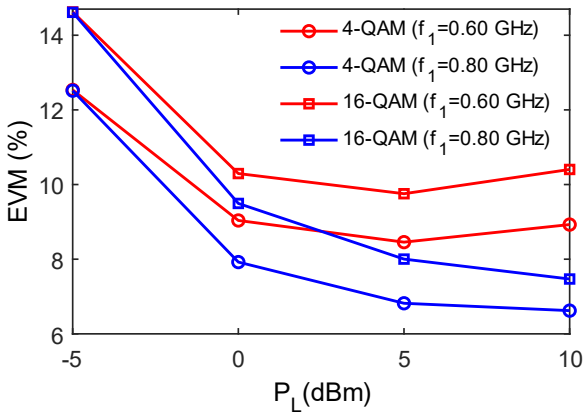

Fig. 10. Average EVM vs P_L with 4-QAM and 16-QAM modulations for two IF configurations.

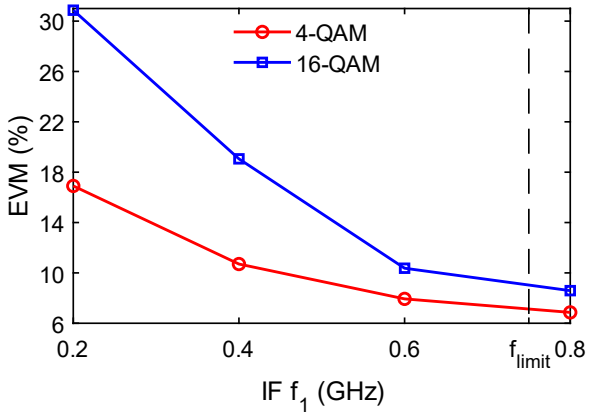

Fig.11. Average EVM with 4-QAM and 16-QAM modulations for different values of the IF f_1 at $P_L = 10$ dBm.

IV. CONCLUSION

In this paper, we proposed an analytical intermediate frequency optimization method in order to mitigate second-order intermodulation distortion products and harmonics induced by the Mach-Zehnder optical modulator, SOA, and photodiode association, in a 5G OFDM system, through the analog optical fronthaul network of the C-RAN. Based on an experimental study of three transmitted OFDM bands of 200 MHz, we proved that our optimized IF configuration prevents second-order interband intermodulation distortion. Indeed, an EVM enhancement is achieved from a certain value of laser power for the 4 and 16-QAM case, while keeping EVM values for all bands practically equal.

REFERENCES

[1] A. Checko, H. L. Christiansen, Y. Yan, L. Scolari, G. Kardaras, M. S. Berger and L. Dittmann, "Cloud RAN for mobile networks—A technology overview", IEEE Communications Surveys & Tutorials, Vol. 17, No. 1, pp. 405-426, 2014.

[2] A. Pizzinat, P. Chanclou, F. Saliou and T. Diallo, "Things you should know about fronthaul", Journal of Lightwave Technology, Vol. 33, No. 5, pp. 1077-1083, 2015.

[3] X. Liu, H. Zeng, N. Chand and F. Effenberger, "Efficient mobile fronthaul via DSP-based channel aggregation", Journal of Lightwave Technology, Vol. 34, No. 6, pp. 1556-1564, 2015.

[4] I. A. Alimi, A. L. Teixeira, P. P. Monteiro, "Toward an efficient C-RAN optical fronthaul for the future networks: A tutorial on technologies, requirements, challenges, and solutions", IEEE Communications Surveys & Tutorials, Vol. 20, No. 1, pp. 708-769, 2017.

[5] P. T. Dat, A. Kanno, N. Yamamoto and T. Kawanishi, "5G transport networks: the need for new technologies and standards", IEEE Communications Magazine, Vol. 54, No. 9, pp. 18-26, 2016.

[6] A. Delmade, C. Browning, A. Farhang, N. Marchetti, L. E. Doyle, D. Koilpillai, L.P. Barry and D. Venkitesh, "Performance analysis of analog IF over fiber fronthaul link with 4G and 5G coexistence", Journal of Optical Communications and Networking, Vol. 10, No. 3, pp. 174-182, 2018.

[7] H. H. Lu, "Performance comparison between DCF and RDF dispersion compensation in fiber optical CATV systems", IEEE Transactions on Broadcasting, Vol. 48, No 4, pp. 370-373, 2002.

[8] J. E Sime, P. Morel, M. Younes, I. S. Stievano, M. Telescu, N. Tanguy and S. Azou, "The Effects of Digital Predistortion in a CO-OFDM System—A Stochastic Approach", IEEE Photonics Technology Letters, vol. 32, no 13, p. 763-766, 2020.

[9] N. P. Diamantopoulos, H. Nishi, W. Kobayashi, K. Takeda, T. Kakitsuka and S. Matsuo, "On the Complexity Reduction of the Second-Order Volterra Nonlinear Equalizer for IM/DD Systems", Journal of Lightwave Technology, Vol. 37, No. 4, pp. 1214-1224, 2019.

[10] I. Ha, H. J. Park and S. K. Han, "Nonlinearity mitigation in multi-IFoF-based mobile fronthaul transmission using spectral power shaping", Optics Communications, Vol. 437, pp. 382-387, 2019.

[11] C. Han, M. Sung, S.H. Cho, H. S. Chung, S. M. Kim and J. H. Lee, "Performance improvement of multi-IFoF-based mobile fronthaul using dispersion-induced distortion mitigation with IF optimization", Journal of Lightwave Technology, Vol. 34, No. 20, pp. 4772-4778, 2016.

[12] M. Sung, S. H. Cho, H. S. Chung, S. M. Kim and J. H. Lee, "Investigation of transmission performance in multi-IFoF based mobile fronthaul with dispersion-induced intermixing noise mitigation", Optics Express, Vol. 25, No 8, pp. 9346-9357, 2017.

[13] European Telecommunications Standards Institute (ETSI), 3rd Generation Partnership Project (3GPP), "5G; NR; Base Station (BS) radio transmission and reception (3GPP TS 38.104 version 15.5.0 Release 15)", 2019.

[14] H. Khaleghi, P. Morel, A. Sharaiha and T. Rampone, "Experimental validation of numerical simulations and performance analysis of a coherent optical-OFDM transmission system employing a semiconductor optical amplifier", Journal of Lightwave Technology, Vol. 31, No. 1, pp. 161-170, 2012.

[15] V. A. Thomas, M. El-Hajjar and L. Hanzo, "Performance improvement and cost reduction techniques for radio over fiber communications", IEEE Communications Surveys & Tutorials, Vol. 17, No. 2, pp. 627-670, 2015.

[16] M. Kasmi, P. Morel, M. Telescu, V. Choqueuse, N. Tanguy and S. Azou, "Influence of frequency mapping on intermodulation distortion in an SOA-based optical fronthaul C-RAN architecture for 5G communications", International Conference on Transparent Optical Networks (ICTON), IEEE, Bucharest, Romania, July 2-6, 2023.